



This is a repository copy of *Antarctic ice sheet sensitivity to atmospheric CO₂ variations in the early to mid-Miocene*.

White Rose Research Online URL for this paper:
<http://eprints.whiterose.ac.uk/98017/>

Version: Submitted Version

Article:

Levy, R., Harwood, D., Florindo, F. et al. (23 more authors) (2016) Antarctic ice sheet sensitivity to atmospheric CO₂ variations in the early to mid-Miocene. *Proceedings of the National Academy of Sciences*, 113 (13). pp. 3453-3458. ISSN 1091-6490

<https://doi.org/10.1073/pnas.1516030113>

Reuse

Unless indicated otherwise, fulltext items are protected by copyright with all rights reserved. The copyright exception in section 29 of the Copyright, Designs and Patents Act 1988 allows the making of a single copy solely for the purpose of non-commercial research or private study within the limits of fair dealing. The publisher or other rights-holder may allow further reproduction and re-use of this version - refer to the White Rose Research Online record for this item. Where records identify the publisher as the copyright holder, users can verify any specific terms of use on the publisher's website.

Takedown

If you consider content in White Rose Research Online to be in breach of UK law, please notify us by emailing eprints@whiterose.ac.uk including the URL of the record and the reason for the withdrawal request.



eprints@whiterose.ac.uk
<https://eprints.whiterose.ac.uk/>

Antarctic Ice Sheet sensitivity to atmospheric CO₂ variations during the early to mid-Miocene

Richard Levy^a, David Harwood^b, Fabio Florindo^c, Francesca Sangiorgi^d, Robert Tripati^e, Hilmar von Eynatten^f, Edward Gasson^g, Gerhard Kuhn^h, Aradhna Tripati^e, Robert DeConto^g, Christopher Fielding^b, Brad Field^a, Nicholas Golledge^{i,a}, Robert McKayⁱ, Timothy Naish^{i,a}, Matthew Olney^j, David Pollard^k, Stefan Schouten^l, Franco Talarico^m, Sophie Warnyⁿ, Veronica Willmott^h, Gary Acton^o, Kurt Panter^p, Timothy Paulsen^q, Marco Taviani^r, and SMS Science Team

^aDepartment of Paleontology, GNS Science, Lower Hutt 5040, New Zealand, Tel: +64 4 570 1444, r.levy@gns.cri.nz ^bDepartment of Earth & Atmospheric Sciences, University of Nebraska-Lincoln, Lincoln, NE 68588-0340, USA, ^cIstituto Nazionale di Geofisica e Vulcanologia, I-00143 Rome, Italy, ^dMarine Palynology and Paleoceanography, Laboratory of Palaeobotany and Palynology, Department of Earth Sciences, Faculty of Geoscience, Utrecht University, 3584 CD, Utrecht, The Netherlands, ^eDepartment of Earth, Planetary, & Space Sciences and Department of Atmospheric & Oceanic Sciences, Institute of the Environment and Sustainability, University of California Los Angeles, Los Angeles, CA 90095, USA, ^fDepartment of Sedimentology & Environmental Geology, Geoscience Center Göttingen (GZG), 37077, Göttingen, Germany, ^gDepartment of Geosciences, University of Massachusetts, Amherst, MA 01003-9297, USA, ^hAlfred Wegener Institute for Polar & Marine Research, 27568, Bremerhaven, Germany, ⁱAntarctic Research Centre, Victoria University of Wellington, Wellington 6012, New Zealand, ^jHillsborough Community College, 10414 E. Columbus Drive, Tampa, FL, USA, ^kEarth & Environmental Systems Institute, Pennsylvania State University, University Park, PA 16802, USA, ^lMarine Organic Biogeochemistry, Royal Netherlands Institute for Sea Research, 1797 SZ 't Horntje (Texel), The Netherlands, ^mDipartimento di Scienze Fisiche, della Terra e dell'Ambiente, Università degli Studi di Siena, Siena, Italy, ⁿDepartment of Geology & Geophysics, and Museum of Natural Science, Louisiana State University, Baton Rouge, Louisiana 70803, USA, ^oDepartment of Geography & Geology, Sam Houston State University, Huntsville, TX 77341, USA, ^pDepartment of Geology, Bowling Green State University, Bowling Green, OH 43403-0211, USA, ^qDepartment of Geology, Harrington Hall, University of Wisconsin – Oshkosh, Oshkosh, WI 54901-8649, USA, ^rInstitute of Marine Sciences - National Research Council, ISMAR-CNR, 40129 Bologna, Italy

Submitted to Proceedings of the National Academy of Sciences of the United States of America

Geological records from the Antarctic margin offer direct evidence of environmental variability at high southern latitudes and provide insight regarding ice sheet sensitivity to past climate change. The early to mid-Miocene (23 to 14 million years ago) is a compelling interval to study as global temperatures and atmospheric CO₂ concentrations were similar to those projected for coming centuries. Importantly, this time interval includes the Miocene Climatic Optimum (MCO), a period of global warmth during which average surface temperatures were 3 to 4°C higher than today. Miocene sediments in the AND-2A drill core from the Western Ross Sea, Antarctica indicate that the Antarctic Ice Sheet (AIS) was highly variable through this key time interval. A multi-proxy dataset derived from the core identifies four distinct environmental “motifs” based on changes in sedimentary facies, fossil assemblages, geochemistry, and paleotemperature. Four major discontinuities in the drill core coincide with regional seismic discontinuities and reflect transient expansion of grounded ice across the Ross Sea. They correlate with major positive shifts in benthic oxygen isotope records and generally coincide with intervals when atmospheric CO₂ concentrations were at or below pre-industrial levels (~280 ppm). Five intervals reflect ice sheet minima and air temperatures warm enough for substantial ice mass loss during episodes of high (~500 ppm) atmospheric CO₂. These new drill core data and associated ice sheet modelling experiments indicate that polar climate and the AIS were highly sensitive to relatively small changes in atmospheric CO₂ during the early to mid-Miocene.

Antarctica | Ice Sheet | Climate Optimum | Ross Sea | Miocene

Introduction

Knowledge regarding Antarctic Ice Sheet (AIS) response to warming climate is of fundamental importance due to the role ice sheets play in global sea level change. Paleoenvironmental records from Earth's past offer a means to examine AIS variability under past climatic conditions that were similar to today and those projected for the next several decades (1, 2). In this respect, the early to mid-Miocene is a compelling interval to study as proxy reconstructions of atmospheric CO₂, albeit uncertain, suggest that concentrations generally varied between pre industrial levels (PAL=280ppm) and values at or above 500ppm (3-9). Additionally, global mean surface temperature during peak Miocene warmth was up to 3 to 4 degrees higher than today (10), similar to

'best-estimate' temperatures expected by 2100 under the highest projected greenhouse gas concentration pathway (RCP 8.5) (1, 2). Finally, Miocene geography was similar to today (11) and major circum-Antarctic oceanic and atmospheric circulation patterns that dominate the modern Southern Ocean were well established (12, 13).

Much of our understanding regarding AIS history through the early to mid-Miocene comes from far field records from deep ocean basins. Benthic oxygen and carbon isotope proxies for global paleoclimate suggest that early to mid-Miocene climate and glacial environments were highly variable (14-19). These records include evidence for major transient glacial episodes and sea level fall, intervals of relative ice sheet stability, and periods of climatic warmth with major ice sheet retreat and sea level rise. Furthermore, reconstructions from sedimentary sequences on the Marion Plateau, offshore NE Australia (20), and New Jersey margin (21) suggest sea level varied by up to 100 m. Episodes of sea level maxima (+40 m) suggest loss of Antarctica's marine-

Significance

New information from the AND-2A drill core and a complementary ice sheet modelling study, show that polar climate and Antarctic Ice Sheet (AIS) margins were highly dynamic during the early to mid-Miocene. Changes in extent of the AIS inferred by these studies suggest that high southern latitudes were sensitive to relatively small changes in atmospheric CO₂ (between 280 and 500 ppm). Importantly, reconstructions through intervals of peak warmth indicate that the AIS retreated beyond its terrestrial margin under atmospheric CO₂ conditions that were similar to those projected for the coming centuries.

Reserved for Publication Footnotes

137
138
139
140
141
142
143
144
145
146
147
148
149
150
151
152
153
154
155
156
157
158
159
160
161
162
163
164
165
166
167
168
169
170
171
172
173
174
175
176
177
178
179
180
181
182
183
184
185
186
187
188
189
190
191
192
193
194
195
196
197
198
199
200
201
202
203
204

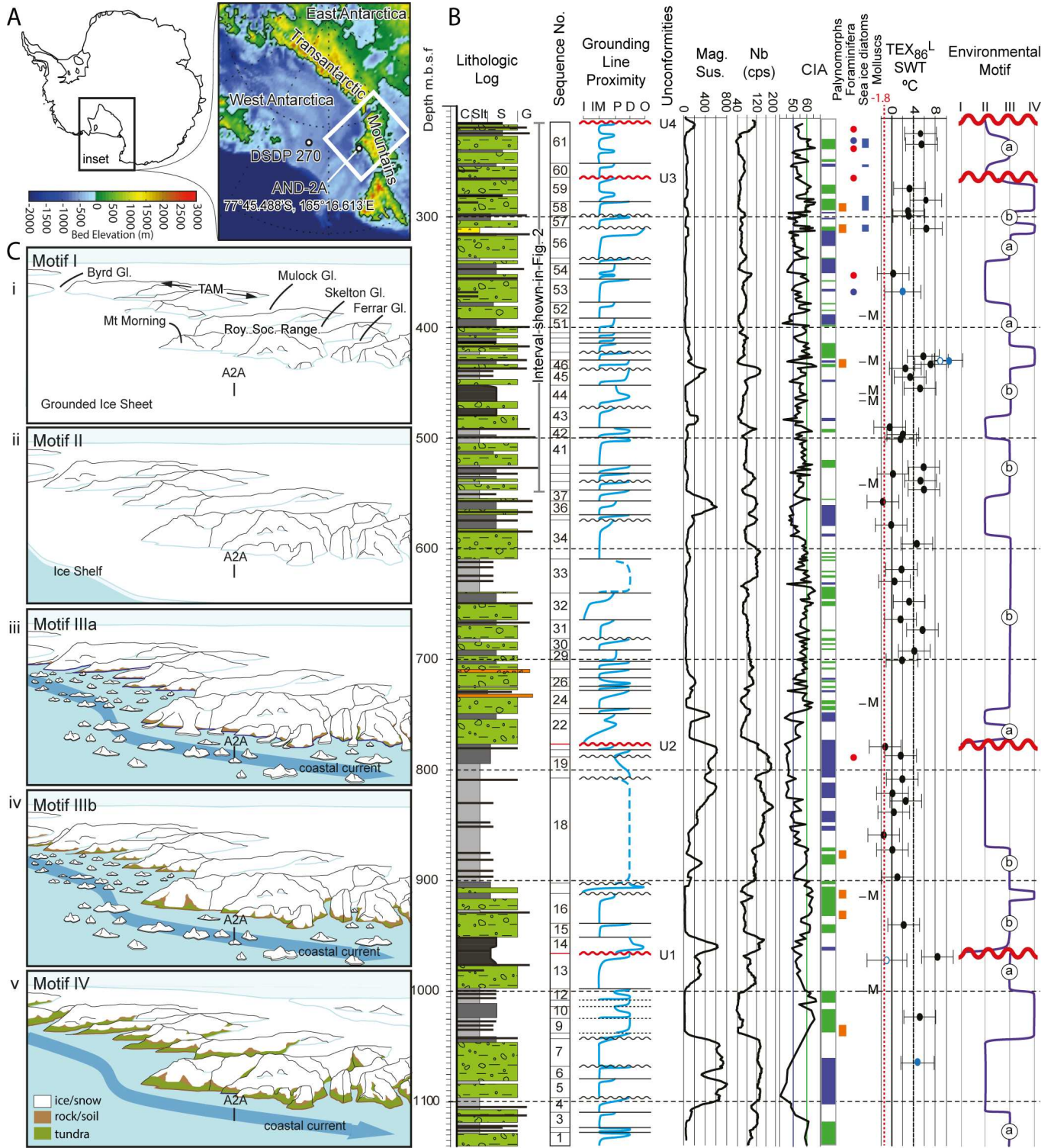


Fig. 1. A. Map showing Ross Sea area (inset) and AND-2A drill site (white box indicates approximate area for schematic reconstructions shown below). B. Stratigraphic summary of lower 925 m of AND-2A (214.13 to 1138.54 mbsf) showing 61 sedimentary cycles. Glacial proximity curve tracks relative position of the grounding line through ice-contact (I), ice-marginal (IM), ice-proximal (P), ice-distal (D) and open marine (O) environments. Continuously acquired data sets include magnetic susceptibility and Niobium (Nb) XRF-CS counts. Chemical Index of Alteration (CIA) (curve and bar) indicates arid (< 50, blue) and less arid (> 60, green) conditions. Intervals of peak palynomorph concentration shown by orange boxes. Foraminifera assemblages include cold water/ice marginal benthic species (red circles) and cool water planktonic species (blue circles). Blue bars = sea-ice diatoms. M=intervals with well-preserved molluscs. Sea water temperature estimates based on TEX_{86}^L (black circles) and Δ_{47} (blue circles, open = less well preserved specimens). Environmental Motif curve based on the proxy environmental data set. C. Schematic reconstructions of region around AND-2A showing likely conditions for each Environmental Motif (I-IV).

based ice sheets that, at present, occupy much of West Antarctica and large portions of East Antarctica (22), as well as substantial loss of mass from Antarctica's terrestrial ice sheets. Episodes

273
274
275
276
277
278
279
280
281
282
283
284
285
286
287
288
289
290
291
292
293
294
295
296
297
298
299
300
301
302
303
304
305
306
307
308
309
310
311
312
313
314
315
316
317
318
319
320
321
322
323
324
325
326
327
328
329
330
331
332
333
334
335
336
337
338
339
340

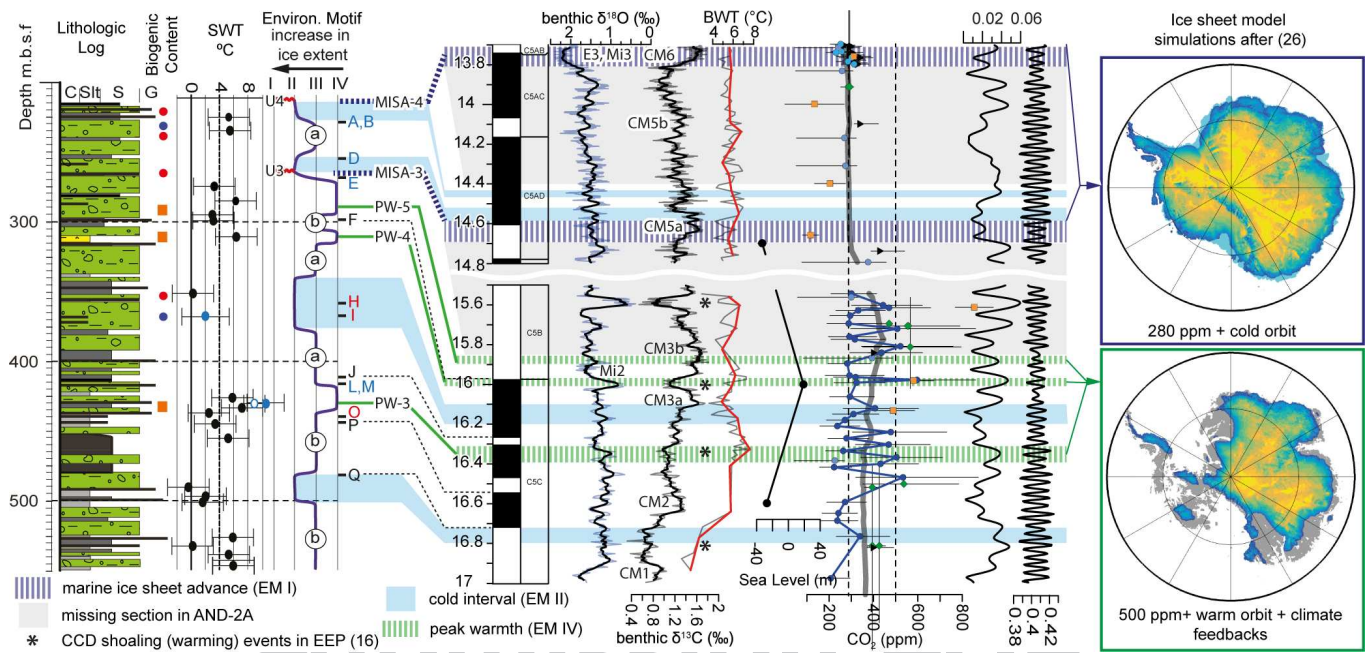


Fig. 2. Mid-Miocene section of AND-2A (557.35 to 214.13 mbsf) correlated to the Geomagnetic Polarity Timescale (46) and selected data sets. See Fig. 1 caption for description of AND-2A data. Letters A-Q indicate position of key age model constraints (see SI text, Fig. S2, and Table S1 for details). Benthic $\delta^{18}\text{O}$ and $\delta^{13}\text{C}$ isotope data with moving averages (thick lines) from IODP Sites U1338 and U1337 (14, 15). Mi events after (19) and E3 oxygen isotope excursion after (16). CM = carbon isotope maxima (18, 39). Asterisks = carbon minima events and intervals of major shoaling of the carbonate compensation depth in the eastern equatorial Pacific (15). Bottom water temperature reconstructions from (17) with 30 pt spline smooth (red line)(note: age model from (17) adjusted by $\sim+50\text{kyrs}$ for section between 15.5 and 17Ma). Sea level data from the Marion Plateau (20). Proxy atmospheric CO_2 data include boron isotopes (3-5) (blue circles), alkenones (3, 6) (black triangles), stomata (7) (green diamonds), and paleosols (orange squares). Thick grey line = 21 point weighted average. Grey shaded 'boxes' = time missing in unconformities; MISA (blue dashed line) = maximum ice sheet advance (EMI); blue shaded 'zones' = cold polar intervals (EMII); PW (green dashed line) = Peak Warm intervals (EMIV). Orbital eccentricity and obliquity from (48). Ice sheet simulations after (25).

of maximum sea level fall (up to -60m) suggest that the AIS occasionally grew and advanced across continental shelves.

Geological records proximal to Antarctica's coastal margin provide direct evidence of past ice sheet variability in response to changing global climate. The AND-2A drill core, a 1,138 meter-long stratigraphic archive of climate and ice sheet variability from the McMurdo Sound sector of the western Ross Sea ($77^{\circ}45.488^{\circ}\text{S}$, $165^{\circ}16.613^{\circ}\text{E}$), was recovered by drilling from an ~ 8.5 m thick floating sea-ice platform in 380 m of water, located ~ 30 kilometres off the coast of Southern Victoria Land (SVL) (Fig. 1A) (23). The drill core comprises lower Miocene to Quaternary glacial-marine strata deposited in the steadily subsiding Victoria Land Basin (VLB)(24). Paleogeography was broadly similar to today although continental shelves in the Ross and Weddell seas were likely shallower (SI text). Recovered core sediments, and proxies they contain, allow us to assess past ice sheet dynamics along a coastal margin influenced by ice flowing from East Antarctica and across the West Antarctic continental shelf. Through analysis of an integrated proxy environmental data set we derive a new environmental reconstruction, and combine this with a suite of global environmental data to establish a history of AIS response to global climate events and episodes during the early to mid-Miocene. This integrated data set allows us to evaluate key drivers of high latitude climate and ice sheet variability between 21 and 13 Ma. Outcomes from research reported here and in a companion ice sheet modelling study (25) suggest the AIS advanced across continental shelves during cold orbital configurations and retreated well inland of the coast under warm orbits. This large range of AIS variability occurred under a relatively low range in atmospheric CO_2 concentration (~ 280 to 500 ppm) and indicates the Antarctic environment was highly sensitive during the early to mid-Miocene.

Results

A near-continuous record spanning 20.2 to ~ 15 Ma is preserved in the lower 925 meters of AND-2A (Figs. 1B; S2; S3; Table S1). A diverse range of geological information including physical properties and sedimentological, paleontological, and geochemical data were collected (summarised in SI text and published (23, 26-33)). Here we present new data including sea surface water (upper 200 m) temperatures (SWTs) derived from archaeal lipids (TEX^1_{86}) and carbonate isotopes (Δ_{47}), whole rock inorganic geochemical data, and an integrated age model, and offer the first analysis of a combined proxy environmental data set derived from AND-2A (Figs. 1B; S3). These paleoenvironmental data are used to define four characteristic environmental motifs (EM) (Table S2) that reflect distinct climatic and glacial regimes (Fig. 1A and B).

Intervals of maximum ice sheet extent and cold polar conditions are assigned to **EM I (maximum ice)** and are characterised in AND-2A by four major disconformities. These disconformities are relatively rare and represent distinct and discrete times of major ice sheet advance beyond the drill site onto the continental shelf (Fig. 1Ci). Three disconformities AND2A-U1 (965.43 meters below sea floor, mbsf); -U2 (774.94 mbsf); and -U3 (262.57 mbsf) span the time intervals ~ 20 to 19.8 Ma, ~ 18.7 to 17.8 Ma, and ~ 15.8 to 14.6 Ma, respectively (Fig. S2). A fourth major disconformity AND2A-U4 (214.13 mbsf) separates middle Miocene rocks ($> \sim 14.4$ Ma, Fig. S2) from 214 meters of overlying upper Miocene to Quaternary strata.

Eight stratigraphic intervals in AND-2A are assigned to **EM II (cold polar)**, as characterised by high magnetic susceptibility (MS), high Niobium (Nb) content, and low Chemical Index of Alteration (CIA), all of which reflect sediment derived from local volcanic centers and unweathered outcrop in proximal regions of the Transantarctic Mountains (TAM). We infer that relative increases in local sediment are due to advance of ice from ex-

341
342
343
344
345
347
348
349
350
351
352
353
354
355
356
357
358
359
360
361
362
363
364
365
366
367
368
369
370
371
372
373
374
375
376
377
378
379
380
381
382
383
384
385
386
387
388
389
390
391
392
393
394
395
396
397
398
399
400
401
402
403
404
405
406
407
408

409 panding ice caps on nearby Mount Morning and the Royal Society
410 Range under a cold polar climate. Five of the eight intervals are
411 dominated by massive to stratified diamictite facies that often
412 contain debris derived from local volcanic sources and were prob-
413 ably deposited beneath a floating ice tongue or ice shelf proximal
414 to the grounding line of outlet or piedmont glaciers (Fig. 1Cii).
415 Each of these intervals is typically fossil-poor. TEX_{86}^L -derived
416 SWT's range between -1.4 and $2.6 \pm 2.8^\circ\text{C}$ and are supported by a
417 Δ_{47} derived value of $2.1 \pm 3.7^\circ\text{C}$ at 366 mbsf. We infer that proxies
418 in EM II reflect cold polar conditions with minimum grounding-
419 line variability and persistent floating ice shelves and/or coastal
420 fast ice.

421 Twelve stratigraphic intervals are assigned to **EM III (cold**
422 **temperate)** as characterised by low to moderate MS, low to
423 moderate Nb content and moderate to high CIA. These data
424 indicate variable sediment provenance and periodic input from
425 local volcanic sources and/or unweathered outcrop. EM III is
426 divided into sub-types 'a' and 'b' based on variations in lithofacies
427 and fossil content. **EM IIIa** is dominated by stratified diamictite
428 and gravel with variable clast composition but including a high
429 proportion of rock fragments sourced from the region south of
430 Skelton and Mulock glaciers. Foraminifera vary in abundance and
431 are absent in many intervals but include up to ten species in others
432 (30). Marine diatoms and terrestrial palynomorphs are usually
433 absent but occur in low abundance in several discrete intervals.
434 Mollusc-bearing intervals are uncommon. TEX_{86}^L -derived SWTs
435 range between 2.2 and $5.4^\circ\text{C} \pm 2.8^\circ\text{C}$. Intervals characterised by
436 EM IIIa likely reflect a sub polar climate and glacial regime with
437 tidewater glaciers. Periodic increase in gravel clasts derived from
438 regions south of Mount Morning reflect an increase in ice flux
439 through major East Antarctic Ice Sheet (EAIS) outlet valleys into
440 fjords under warmer conditions. During these intervals, calving
441 rates at the grounding-line increased and debris-laden icebergs
442 delivered sediment to the drill site as they drifted northwards
443 along the SVL coast (Fig. 1Ciii).

444 **EM IIIb** has persistently low Nb and MS, reflecting minimal
445 input from local volcanic sources. Lithofacies are diverse and
446 include massive and stratified diamictite and gravel; clast com-
447 position is mixed, with a high proportion of lithologies derived
448 from the Skelton and Mulock glaciers and as far south as the
449 Carlyon and Byrd glaciers. Intervals of mudrock dominated se-
450 quences are more common in EM IIIb than in EM IIIa. Terrestrial
451 palynomorphs are more abundant in several intervals of EM IIIb
452 (e.g., 947.54; 922.61; and 593.29 mbsf) and discrete intervals
453 bearing mollusc fossils occur occasionally (Figs. 1B; S3). TEX_{86}^L -
454 derived SWTs range from 0.2 to $6.7^\circ\text{C} \pm 2.8^\circ\text{C}$. We infer that EM
455 IIIb reflects a depositional setting similar to EM IIIa but with a
456 generally warmer climate, particularly during periods when SWTs
457 were $6-7^\circ\text{C} \pm 2.8^\circ\text{C}$ and local ice cap margins retreated to the coast
458 and had limited influence on marine sedimentation at the drill
459 site. Coarse clastic sediment was primarily delivered to the drill
460 site by debris-rich icebergs derived from large fast flowing outlet
461 glaciers to the south. Increased abundance of *Podocarpites* spp.
462 and *Nothofagidites* spp. pollen (Figs. 1B; S3) indicates local tundra
463 occupied ice-free regions along the coastal margin (Fig. 1Civ).

464 Five relatively short, lithologically diverse, stratigraphic inter-
465 vals are assigned to **EM IV (minimum ice)** as characterised by
466 low MS, low Nb content and high CIA, which indicate minimal
467 sediment input from local volcanic sources and/or unweathered
468 outcrop. Lithofacies are variable but sequences are usually domi-
469 nated by mudrock, sandstone, and thin diamictite. A 46 meter-
470 thick section between 996.69 and 1042.55 mbsf incorporates five
471 sequences dominated by sediments deposited within a marine-
472 deltaic setting distal to the glacial margin (27). The interval
473 between 428.28 and 436.18 mbsf incorporates a single sequence
474 comprising a basal diamictite overlain by a sandstone unit with
475 relatively abundant marine bivalves. Thick-shelled costate scal-

476 lops as well as venerid clams recovered from this interval indicate
477 that water temperatures were at least 5°C warmer than in the
478 Ross Sea today (29). Relatively warm water temperatures are
479 supported by TEX_{86}^L and Δ_{47} data, which indicate SWT at the
480 coastal margin reached a maximum between $7.0 \pm 2.8^\circ\text{C}$ and 10.4
481 $\pm 2.5^\circ\text{C}$. *In-situ* pollen and spores are abundant in this interval
482 and indicate a coastal vegetation of mossy tundra with shrub
483 podocarps and southern beech and suggest a cool terrestrial
484 climate (10°C January mean air temperature) (31-33). Evidence
485 for another interval of 'warm' climate is also preserved in a unique
486 diatom-rich unit at ~ 310 mbsf. This unit contains a 'typical'
487 tundra pollen assemblage recovered from other EM IV units but
488 also includes freshwater algae and cosmopolitan dinoflagellate
489 taxa that indicate much warmer temperatures than occur in the
490 Ross Sea today (32). Furthermore, TEX_{86}^L analyses from the
491 diatomite unit indicate maximum surface water temperatures of
492 ~ 6 to $7^\circ\text{C} \pm 2.8^\circ\text{C}$, which is consistent with values inferred from
493 the fossils (29, 32) (SI text). EM IV records times when the AIS
494 margin retreated well inland and tundra occupied ice free regions
495 from the coast to at least 80 km inland (34)(Fig. 1Cv).

496 Discussion

497 Proxy environmental data derived from AND-2A indicate coastal
498 environments in SVL were highly variable throughout the early to
499 mid-Miocene (Figs. 1B; 1C). A robust age model for the AND-
500 2A core (see methods and SI text) allows us to integrate envi-
501 ronmental data from the Antarctic coastal margin with regional
502 seismic data from the Ross Sea continental shelf (35), deep sea
503 oxygen and carbon isotope data (14, 15), sea level records (20),
504 and atmospheric CO_2 reconstructions (3-9)(Figs. 2; S5). We ac-
505 knowledge that the age model for each data set has uncertainties
506 and caution that both proxy CO_2 reconstructions and sea level
507 records are presently limited in temporal resolution and subject
508 to large uncertainties. Despite these limitations, our correlation
509 framework (Figs. 2; S5) highlights several distinct episodes of:
510 (1) cold climate and marine-based ice sheet advance, (2) peak
511 warmth and maximum ice sheet retreat, and (3) cold climate with
512 relatively stable terrestrial ice sheets, which are discussed in detail
513 below.

514 Four episodes of Maximum Ice Sheet Advance in the Ross
515 Sea (MISA-1 to MISA-4) are documented between 21 and 13
516 Ma (Figs. 2; S5). MISA episodes are recorded by stratigraphic
517 gaps in AND-2A that correlate approximately in time with one
518 of the major Ross Sea Unconformities (RSU's) that formed
519 during ice sheet advance across the continental shelf (35). Each
520 MISA episode also correlates generally with an interval of global
521 sea level fall, enrichment in deep-sea benthic $\delta^{18}\text{O}$, increase in
522 benthic $\delta^{13}\text{C}$ values, and decrease in bottom water temperature
523 (BWT) (Figs. 2; S5). These patterns suggest episodes of maxi-
524 mum ice sheet advance were not restricted to the Ross Sea but
525 represent continental scale expansion of the AIS. Importantly,
526 our correlation model suggests that these MISA episodes co-
527 incided generally with eccentricity minima and intervals when
528 atmospheric CO_2 concentrations were below 300 ppm (4, 5).
529 MISA-3 ($\sim 14.6 - 14.7$ Ma) best illustrates these associations (Fig.
530 2) and is characterised by a ~ 30 m drop in sea level (20), a 2
531 to 3°C decrease in BWT in the Southern Ocean (17), a 0.75‰
532 enrichment in $\delta^{18}\text{O}$, a major increase in $\delta^{13}\text{C}$ (CM 5 of (18)) and
533 a decrease in atmospheric CO_2 concentration to ~ 300 ppm (4,
534 5). MISA-4 ($\sim 13.7 - 14.1$ Ma)(Fig. S5) coincides with the major
535 Mi-3/E3 oxygen isotope excursion (16, 19), a drop in sea level of
536 ~ 60 m (20), a 2 to 3°C decrease in BWT (17), and a drop in CO_2
537 below 300 ppm (3, 5)(Fig. 2; Fig. S5). MISA-3 and -4 correspond
538 in time with RSU 4, a surface that displays erosional features
539 with relief similar to bathymetric troughs that formed beneath
540 ice streams during recent glaciations (36). RSU 4 likely formed
541 during a phase of ice sheet advance and retreat that began ~ 14.6
542
543
544

Ma and culminated in the Miocene Climate Transition (MCT) and maximum ice sheet advance at 13.8 Ma. This phase of cold climate and persistent marine based ice sheets ended at ~10 Ma when ice retreated to the terrestrial margins as revealed by upper Miocene mud-rich sediments in AND-1B (37).

Five episodes of Peak Warmth (PW-1 to PW-5), during which AIS grounding-lines retreated inland of the coastal margin, are also recorded. PW episodes are characterised by warm climate indicators in AND-2A (EM IV) that coincide generally with times of elevated BWT, depleted $\delta^{18}\text{O}$ values, eccentricity maxima, low $\delta^{13}\text{C}$ values, and relatively high atmospheric CO_2 concentrations (Figs. 2; S5). Intervals PW-3, -4, and -5 occurred between 16.4 and 15.8 Ma (Fig. 2) and offer insight into AIS response during the MCO. Ice-distal sediments in these intervals are relatively rich in terrestrial palynomorphs, and proxies indicate that SWTs in the Ross Sea were 6–10°C warmer than today. PW-4 (16 Ma) best illustrates these relationships as it correlates with a major (~0.5‰) decrease in $\delta^{18}\text{O}$, a 0.4‰ decrease in $\delta^{13}\text{C}$, a 2 to 3°C increase in BWT at ODP Site 1171 (17), and a 10 to 20 m rise in sea level across the Marion Plateau (20). Importantly, proxy data show that atmospheric CO_2 concentrations were >500 ppm during this warm episode (4, 7) (Fig. 2), which suggests that high latitude climate and Antarctica's terrestrial ice sheets were sensitive to CO_2 levels much lower than climate models suggest (38).

An unusual period of cold and relatively stable climate is suggested by proxies in the prominent thick interval of fine-grained sediments between 901.54 to 774.94 mbsf in AND-2A (Sequence 18, Fig. 1B; S3). This unique stratigraphic interval is characterised by very low amounts of pollen and spores and persistently low SWTs (-1.3 to 2.6°C). Foraminifera and diatoms are rare to absent. We infer the mudstone accumulated in a dark environment beneath semi-permanent sea ice or an ice shelf. Interestingly, this interval correlates to upper Chron C6n, a time interval characterised by stable sea level (21) and low variability in orbital eccentricity (Fig. S2). Collectively these data suggest that global climate and the AIS remained relatively stable through several glacial-interglacial cycles spanning at least 500 kyrs.

We conclude that environmental data from AND-2A and key far-field records suggest that Antarctica's climate and ice sheets were highly variable during the early to mid-Miocene. Whereas orbital variations were the primary driver of glacial cycles (28, 33, 39), atmospheric CO_2 variations modulated the extent of ice sheet advance and retreat. Specifically, coldest conditions and maximum ice sheet growth (MISA episodes and EM II) occurred generally during eccentricity minima and when atmospheric CO_2 was low (<400 ppm). Peak warmth and maximum AIS retreat occurred during eccentricity maxima and intervals of high CO_2 (≥ 500 ppm). Numerical climate and ice sheet model simulations produced in our companion study (25) (Fig. 2) support these observations and simulate grounding line advance across Antarctica's continental shelves under cold orbits and low CO_2 (280 ppm) but maximum retreat under warm orbital configuration and high CO_2 (500 ppm). Together, these studies suggest that polar climate and the AIS were highly sensitive to relatively small changes in atmospheric CO_2 during the early to mid-Miocene.

Summary

Our analysis of the AND-2A drill core and synthesis with regional and global data show that the early to mid-Miocene Antarctic coastal climate was highly variable. During relatively short-lived intervals of peak warmth summer land surface air temperature was at least 10°C, tundra vegetation extended to

locations 80 km inland (34, 40), surface water temperatures in the Ross Sea were between 6 and 10°C, and the AIS retreated inland. During intermittent intervals of peak cold climate, vegetation vanished and the AIS grew and advanced into the marine environment, expanding across the continental shelf.

Whereas glacial cycles were paced by orbital variability through the early to mid-Miocene, maximum ice sheet retreat occurred when atmospheric CO_2 was ≥ 500 ppm and maximum advance when CO_2 was ≤ 280 ppm (Figs. 2; S5) (4). New numerical ice sheet simulations (25) also show that the Miocene AIS expanded across the continental shelf when atmospheric CO_2 was low (280 ppm) and retreated well inland of the coast when CO_2 was high (500 ppm). These ice sheet proximal data and model simulations support inferences from benthic deep sea records that suggest the global climate system and AIS were highly sensitive during the mid-Miocene (14–16). These results are consistent with observations and numerical climate and ice sheet simulations based on the warm Pliocene (41–44), which indicate that sustained levels of atmospheric $\text{CO}_2 > 400$ ppm may represent a stability threshold for marine-based portions of the West and East Antarctic ice sheets. Furthermore, outcomes from our complementary drill core analysis and ice sheet modelling indicate that Antarctica's terrestrial ice sheets were vulnerable when atmospheric CO_2 concentrations last exceeded 500 ppm. Given current atmospheric CO_2 levels have risen above 400 ppm (45) and are projected to go higher (2), paleoclimate reconstructions such as this one for the early to mid-Miocene imply an element of inevitability to future polar warming, Antarctic ice sheet retreat, and sea level rise.

Methods and Materials

Methods are presented in detail in SI text and (23). AND-2A was described using standard sedimentological techniques to produce detailed stratigraphic logs (27). An age model for the core (SI text, Fig. S2) utilises magnetostratigraphy, biostratigraphy, $^{87}\text{Sr}/^{86}\text{Sr}$ dating of macrofossils, and ^{40}Ar - ^{39}Ar ages on lava clasts and tephra layers to correlate rock units to the Global Polarity Timescale (46). Assemblages of fossil pollen, dinoflagellates, diatoms, foraminifera, and molluscs were used to constrain paleoenvironmental conditions. A standard suite of continuous physical properties was collected on whole and split core and in the borehole. Whole rock inorganic geochemical data were collected at high sampling resolution using an X-ray fluorescence core scanner (XRF-CS). Additional chemical data were collected from discrete bulk sediment samples at lower resolution to provide calibration points for near-continuous non-invasive sampling obtained via XRF-CS. Concentrations of Al_2O_3 , Na_2O , CaO , K_2O , P_2O_5 , and total organic carbon (TOC) from bulk sediment samples were used to calculate the CIA (47). Samples for TEX^L_{86} were prepared at Utrecht University and LC-MS analyses performed at the Royal Netherlands Institute for Sea Research. Samples for Δ_{47} (clumped isotopes) were prepared and analysed at the California Institute of Technology.

Acknowledgements.

Authors thank three anonymous reviewers. We acknowledge the AN-DRILL Program, which acquired the unique geological section examined in this study. Scientific research was supported by the NZ Ministry of Business Innovation and Employment contracts C05X0410 and C05X1001, US National Science Foundation (Cooperative Agreement no. 0342484 to the University of Nebraska—Lincoln), the Italian Antarctic Research Programme, the German Research Foundation (DFG), the Alfred Wegener Institute for Polar and Marine Research (Helmholtz Association of German Research Centres), and New Zealand Antarctic Research Institute grant NZARI 2013 – 1.

1. IPCC (2013) Climate Change 2013: The Physical Science Basis. *Contribution of Working Group I to the Fifth Assessment Report Intergovernmental Panel on Climate Change*, (Cambridge University Press).
2. Meinshausen M, et al. (2011) The RCP greenhouse gas concentrations and their extensions from 1765 to 2300. *Climatic Change* 109(1-2):213-241.

3. Badger MPS, et al. (2013) CO_2 drawdown following the middle Miocene expansion of the Antarctic Ice Sheet. *Paleoceanography* 28(1):42-53.
4. Greenop R, Foster GL, Wilson PA, & Lear CH (2014) Middle Miocene climate instability associated with high-amplitude CO_2 variability. *Paleoceanography* 29(9):2014PA002653.
5. Foster GL, Lear CH, & Rae JWB (2012) The evolution of p CO_2 , ice volume and climate

681
682
683
684
685
686
687
688
689
690
691
692
693
694
695
696
697
698
699
700
701
702
703
704
705
706
707
708
709
710
711
712
713
714
715
716
717
718
719
720
721
722
723
724
725
726
727
728
729
730
731
732
733
734
735
736
737
738
739
740
741
742
743
744
745
746
747
748

- during the middle Miocene. *Earth and Planetary Science Letters* 341–344(0):243-254.
6. Zhang YG, Pagani M, Liu Z, Bohaty SM, & DeConto R (2013) A 40-million-year history of atmospheric CO₂. *Philosophical Transactions of the Royal Society A: Mathematical, Physical and Engineering Sciences* 371(2001).
7. Kürschner WM, Kvaček Z, & Dilcher DL (2008) The impact of Miocene atmospheric carbon dioxide fluctuations on climate and the evolution of terrestrial ecosystems. *Proceedings of the National Academy of Sciences* 105(2):449-453.
8. Retallack GJ (2009) Greenhouse crises of the past 300 million years. *Geological Society of America Bulletin* 121(9-10):1441-1455.
9. Ekart DD, Cerling TE, Montanez IP, & Tabor NJ (1999) A 400 million year carbon isotope record of pedogenic carbonate; implications for paleoatmospheric carbon dioxide. *American Journal of Science* 299(10):805-827.
10. You Y, Huber M, Müller RD, Poulsen CJ, & Ribbe J (2009) Simulation of the Middle Miocene Climate Optimum. *Geophysical Research Letters* 36:1-5.
11. Herold N, Seton M, Müller RD, You Y, & Huber M (2008) Middle Miocene tectonic boundary conditions for use in climate models. *Geochem. Geophys. Geosyst.* 9(10):Q10009.
12. Herold N, Huber M, & Müller RD (2011) Modeling the Miocene Climatic Optimum. Part I: Land and Atmosphere*. *Journal of Climate* 24(24):6353-6372.
13. Herold N, Huber M, Müller RD, & Seton M (2012) Modeling the Miocene climatic optimum: Ocean circulation. *Paleoceanography* 27(1):PA1209.
14. Holbourn A, et al. (2014) Middle Miocene climate cooling linked to intensification of eastern equatorial Pacific upwelling. *Geology* 42(1):19-22.
15. Holbourn A, Kuhnt W, Kochhann KGD, Andersen N, & Sebastian Meier KJ (2015) Global perturbation of the carbon cycle at the onset of the Miocene Climatic Optimum. *Geology* 43(2):123-126.
16. Flower BP & Kennett JP (1993) Middle Miocene ocean-climate transition; high-resolution oxygen and carbon isotopic records from Deep Sea Drilling Project Site 588A, Southwest Pacific. *Paleoceanography* 8(6):811-843.
17. Shevenell AE, Kennett JP, & Lea DW (2008) Middle Miocene ice sheet dynamics, deep-sea temperatures, and carbon cycling: A Southern Ocean perspective. *Geochem. Geophys. Geosyst.* 9(2):Q02006.
18. Woodruff F & Savin S (1991) Mid-Miocene Isotope Stratigraphy in the Deep Sea: High-Resolution Correlations, Paleoclimatic Cycles, and Sediment Preservation. *Paleoceanography* 6(6):755-806.
19. Miller KG, Wright JD, & Faribanks RG (1991) Unlocking the ice house: Oligocene-Miocene oxygen isotopes, eustasy, and margin erosion. *Journal of Geophysical Research* 96(B4):6829-6848.
20. John CM, et al. (2011) Timing and magnitude of Miocene eustasy derived from the mixed siliciclastic-carbonate stratigraphic record of the northeastern Australian margin. *Earth and Planetary Science Letters* 304(3-4):455-467.
21. Kominz MA, et al. (2008) Late Cretaceous to Miocene sea-level estimates from the New Jersey and Delaware coastal plain cores: an error analysis. *Basin Research* 20:211-226.
22. Fretwell P, et al. (2013) Bedmap2: improved ice bed, surface and thickness datasets for Antarctica. *The Cryosphere* 7(1):375-393.
23. Harwood D, Florindo F, Talarico F, & Levy RH eds (2008-2009) *Studies from the ANDRILL Southern McMurdo Sound Project, Antarctica - Initial Science Report on AND-2A*, Vol 15(1), p 235.
24. Fielding CR, Whittaker J, Henrys SA, Wilson TJ, & Naish TR (2008) Seismic facies and stratigraphy of the Cenozoic succession in McMurdo Sound, Antarctica: implications for tectonic, climatic and glacial history. *Palaogeography, Palaeoclimatology, Palaeoecology* 260:8-29.
25. Gasson E, DeConto R, Pollard D, & Levy R (submitted) A dynamic Antarctic Ice Sheet in the early to middle Miocene. *Proceedings of the National Academy of Sciences*.
26. Passchier S, et al. (2011) Early and middle Miocene Antarctic glacial history from the sedimentary facies distribution in the AND-2A drill hole, Ross Sea, Antarctica. *Geological Society of America Bulletin*:B30334.30331.
27. Fielding CR, et al. (2011) Sequence stratigraphy of the ANDRILL AND-2A drillcore, Antarctica: A long-term, ice-proximal record of Early to Mid-Miocene climate, sea-level and glacial dynamism. *Palaogeography, Palaeoclimatology, Palaeoecology* 305(1-4):337-351.
28. Passchier S, Falk CJ, & Florindo F (2013) Orbitally paced shifts in the particle size of Antarctic continental shelf sediments in response to ice dynamics during the Miocene climatic optimum. *Geosphere* 9(1):54-62.
29. Beu A & Taviani M (2013) Early Miocene Mollusca from McMurdo Sound, Antarctica (ANDRILL 2A drill core), with a review of Antarctic Oligocene and Neogene Pectinidae (Bivalvia). *Palaentology* 57(2):299-342.
30. Patterson MO & Ishman SE (2012) Neogene benthic foraminiferal assemblages and paleoenvironmental record for McMurdo Sound, Antarctica. *Geosphere* 8(6):1331-1341.
31. Feakins SJ, Warny S, & Lee J-E (2012) Hydrologic cycling over Antarctica during the middle Miocene warming. *Nature Geosci* 5(8):557-560.
32. Warny S, et al. (2009) Palynomorphs from a sediment core reveal a sudden remarkably warm Antarctica during the middle Miocene. *Geology* 37(10):955-958.
33. Griener KW, Warny S, Askin R, & Acton G (2015) Early to middle Miocene vegetation history of Antarctica supports eccentricity-paced warming intervals during the Antarctic icehouse phase. *Global and Planetary Change* 127(0):67-78.
34. Lewis AR & Ashworth AC (2015) An early to middle Miocene record of ice-sheet and landscape evolution from the Friis Hills, Antarctica. *Geological Society of America Bulletin*.
35. De Santis L, Anderson JB, Brancolini G, & Zayatz I (1995) Seismic record of Late Oligocene through Miocene glaciation on the central and eastern Continental shelf of the Ross Sea. *Geology and Seismic Stratigraphy of the Antarctic Margin*, Antarct. Res. Ser., (AGU, Washington, DC), Vol 68, pp 235-260.
36. Anderson JB & Bartek LR (1992) Cenozoic glacial history of the Ross Sea revealed by intermediate resolution seismic reflection data combined with drill site information. *The Antarctic Paleoenvironment: A perspective on global change*, Antarctic Res. Ser., eds Kennett JP & Warnke DA (Amer. Geophys. Union, Washington, D.C.), Vol 56, pp 231-263.
37. McKay R, et al. (2009) The stratigraphic signature of the late Cenozoic Antarctic Ice Sheets in the Ross Embayment. *Geological Society of America Bulletin* 121(11-12):1537-1561.
38. Goldner A, Herold N, & Huber M (2014) The challenge of simulating the warmth of the mid-Miocene climatic optimum in CESM1. *Clim. Past* 10(2):523-536.
39. Holbourn A, Kuhnt W, Schulz M, & Erlenkeuser H (2005) Impacts of orbital forcing and atmospheric carbon dioxide on Miocene Ice Sheet expansion. *Nature* 438:483-487.
40. Lewis AR, et al. (2008) Mid-Miocene cooling and the extinction of tundra in continental Antarctica. *Proceedings of the National Academy of Sciences* 105(31):10676-10680.
41. Naish T, et al. (2009) Obliquity-paced Pliocene West Antarctic ice sheet oscillations. *Nature* 458(7236):322-328.
42. Cook CP, et al. (2013) Dynamic behaviour of the East Antarctic ice sheet during Pliocene warmth. *Nature Geoscience* 6:765-769.
43. Pollard D & DeConto RM (2009) Modelling West Antarctic ice sheet growth and collapse through the past five million years. *Nature* 458:329-332.
44. Pollard D, DeConto RM, & Alley RB (2015) Potential Antarctic Ice Sheet retreat driven by hydrofracturing and ice cliff failure. *Earth and Planetary Science Letters* 412(0):112-121.
45. Tans P (2014) Atmospheric CO₂, Mauna Loa Observatory. ed USA NOAAAN.
46. Ogg JG (2012) Chapter 5 - Geomagnetic Polarity Time Scale. *The Geologic Time Scale*, eds Gradstein FM, Schmitz JGOD, & Ogg GM (Elsevier, Boston), pp 85-113.
47. Nesbitt HW & Young GM (1982) Early Proterozoic climates and plate motions inferred from major element chemistry of lites. *Nature* 299(5885):715-717.
48. Laskar J, Fienga A, Gastineau M, & Manche H (2011) La2010: a new orbital solution for the long-term motion of the Earth. *Astronomy & Astrophysics* 532:15.
49. Wilson DS, et al. (2012) Antarctic Topography at the Eocene-Oligocene Boundary. *Palaogeography, Palaeoclimatology, Palaeoecology* 335-336:24-34.
50. Sugden D & Denton G (2004) Cenozoic landscape evolution of the Convoy Range to Mackay Glacier area, Transantarctic Mountains; onshore to offshore synthesis. *Geological Society of America Bulletin* 116(7-8):840-857.
51. Levy RH, et al. (2012) Late Neogene climate and glacial history of the Southern Victoria Land coast from integrated drill core, seismic and outcrop data. *Global and Planetary Change* 80-81 Special Issue:61-84.
52. Fitzgerald PG (1992) The Transantarctic Mountains of southern Victoria Land: the application of apatite fission track analysis to a rift shoulder uplift. *Tectonics* 11(3):634-662.
53. Kyle PR & Muncy HL (1989) Geology and geochronology of McMurdo Volcanic Group rocks in the vicinity of Lake Morning, McMurdo Sound, Antarctica. *Antarctic Science* 1(04):345-350.
54. Marcano MC, et al. (2009) Chronostratigraphic and paleoenvironmental constraints derived from the 87Sr/86Sr signal of Miocene bivalves, Southern McMurdo Sound, Antarctica. *Global and Planetary Change* 69(3):124-132.
55. Di Vincenzo G, Bracciali L, Del Carlo P, Panter K, & Rocchi S (2009) 40Ar-39Ar dating of volcanogenic products from the AND-2A core (ANDRILL Southern McMurdo Sound Project, Antarctica): correlations with the Erebus Volcanic Province and implications for the age model of the core. *Bulletin of Volcanology* 72:487-505.
56. Florindo F, et al. (2013) Paleomagnetism and biostratigraphy of sediments from Southern Ocean ODP Site 744 (southern Kerguelen Plateau): Implications for early-to-middle Miocene climate in Antarctica. *Global and Planetary Change* 110, Part C(0):434-454.
57. Talarico FM & Sandroni S (2011) Early Miocene basement clasts in ANDRILL AND-2A core and their implications for paleoenvironmental changes in the McMurdo Sound region (western Ross Sea, Antarctica). *Global and Planetary Change* 78(1-2):23-35.
58. Hauptvogel DW & Passchier S (2012) Early-Middle Miocene (17-14 Ma) Antarctic ice dynamics reconstructed from the heavy mineral provenance in the AND-2A drill core, Ross Sea, Antarctica. *Global and Planetary Change* 82-83:38-50.
59. Roser BP & Pyne AR (1989) Whole-rock geochemistry. *Antarctic Cenozoic History from the CIROS-1 Drillhole, McMurdo Sound, DSIR Bulletin*, ed Barrett PJ (DSIR Publishing, Wellington), Vol 245, pp 175-184.
60. Bahlbürg H & Dobrzinski N (2011) Chapter 6: A review of the Chemical Index of Alteration (CIA) and its application to the study of Neoproterozoic glacial deposits and climate transitions. *Geological Society, London, Memoirs* 36(1):81-92.
61. Schouten S, Hopmans EC, Schefuß E, & Sinninghe-Damst JS (2002) Distributional variations in marine crenarchaeotal membrane lipids: a new tool for reconstructing ancient sea water temperatures. *Earth and Planetary Science Letters* 204:265-274.
62. Kim J-H, et al. (2010) New indices and calibrations derived from the distribution of crenarchaeal isoprenoid tetraether lipids: Implications for past sea surface temperature reconstructions. *Geochimica et Cosmochimica Acta* 74(16):4639-4654.
63. Kim J-H, et al. (2012) Holocene subsurface temperature variability in the eastern Antarctic continental margin. *Geophysical Research Letters* 39(6):L06705.
64. Kalanetra KM, Bano N, & Hollibaugh JT (2009) Ammonia-oxidizing Archaea in the Arctic Ocean and Antarctic coastal waters. *Environmental Microbiology* 11(9):2434-2445.
65. Tierney JE & Tingley MP (2014) A Bayesian, spatially-varying calibration model for the TEX86 proxy. *Geochimica et Cosmochimica Acta* 127:83-106.
66. Hopmans EC, et al. (2004) A novel proxy for terrestrial organic matter in sediments based on branched and isoprenoid tetraether lipids. *Earth and Planetary Science Letters* 224(1-2):107-116.
67. Eagle RA, et al. (2013) The influence of temperature and seawater carbonate saturation state on 13C-18O bond ordering in bivalve mollusks. *Biogeosciences* 10(7):4591-4606.
68. Kim ST & O'Neil JR (1997) Equilibrium and non-equilibrium oxygen isotope effects in synthetic carbonates. *Geochimica, Cosmochimica Acta* 61:3461-3475.
69. Marcano MC, Frank TD, Mukasa SB, Lohmann KC, & Taviani M (2015) Diagenetic incorporation of Sr into aragonitic bivalve shells: implications for chronostratigraphic and paleoenvironmental interpretations. *The Depositional Record* 1(1):38-52.
70. Frank TD, Gui Z, & ANDRILL.SMS.Science.Team (2010) Cryogenic origin for brine in the subsurface of southern McMurdo Sound, Antarctica. *Geology* 38(7):587-590.
71. Liebrand D, et al. (2011) Antarctic ice sheet and oceanographic response to eccentricity forcing during the early Miocene. *Clim. Past* 7(3):869-880.

749
750
751
752
753
754
755
756
757
758
759
760
761
762
763
764
765
766
767
768
769
770
771
772
773
774
775
776
777
778
779
780
781
782
783
784
785
786
787
788
789
790
791
792
793
794
795
796
797
798
799
800
801
802
803
804
805
806
807
808
809
810
811
812
813
814
815
816